Auxin transport sites are visualized in planta using fluorescent auxin analogs

Ken-ichiro Hayashi[a,1], Shouichi Nakamura[a], Shiho Fukunaga[a], Takeshi Nishimura[b], Mark K. Jenness[c], Angus S. Murphy[c], Hiroyasu Motose[d], Hiroshi Nozaki[a], Masahiko Furutani[e], and Takashi Aoyama[f]

[a]Department of Biochemistry, Okayama University of Science, Okayama 700-0005, Japan; [b]Department of Biological Sciences, Tokyo Metropolitan University, Tokyo 192-0397, Japan; [c]Department of Plant Science and Landscape Architecture, University of Maryland, College Park, MD 20742; [d]Division of Bioscience, Graduate School of Natural Science and Technology, Okayama University, Okayama 700-8530, Japan; [e]Graduate School of Biological Sciences, Nara Institute of Science and Technology, Nara 630-0192, Japan; and [f]Institute for Chemical Research, Kyoto University, Kyoto 611-0011, Japan

Edited by Mark Estelle, University of California, San Diego, La Jolla, CA, and approved June 23, 2014 (received for review May 17, 2014)

The plant hormone auxin is a key morphogenetic signal that controls many aspects of plant growth and development. Cellular auxin levels are coordinately regulated by multiple processes, including auxin biosynthesis and the polar transport and metabolic pathways. The auxin concentration gradient determines plant organ positioning and growth responses to environmental cues. Auxin transport systems play crucial roles in the spatiotemporal regulation of the auxin gradient. This auxin gradient has been analyzed using SCF-type E3 ubiquitin-ligase complex-based auxin biosensors in synthetic auxin-responsive reporter lines. However, the contributions of auxin biosynthesis and metabolism to the auxin gradient have been largely elusive. Additionally, the available information on subcellular auxin localization is still limited. Here we designed fluorescently labeled auxin analogs that remain active for auxin transport but are inactive for auxin signaling and metabolism. Fluorescent auxin analogs enable the selective visualization of the distribution of auxin by the auxin transport system. Together with auxin biosynthesis inhibitors and an auxin biosensor, these analogs indicated a substantial contribution of local auxin biosynthesis to the formation of auxin maxima at the root apex. Moreover, fluorescent auxin analogs mainly localized to the endoplasmic reticulum in cultured cells and roots, implying the presence of a subcellular auxin gradient in the cells. Our work not only provides a useful tool for the plant chemical biology field but also demonstrates a new strategy for imaging the distribution of small-molecule hormones.

auxin transporter | subcellular localization

The plant hormone auxin plays a pivotal role in embryogenesis, vascular tissue differentiation, tropic responses to light and gravity, and the lateral branching of shoots and roots. Plants establish auxin gradients in response to light, gravity, and touch stimuli that direct tropic growth to allow plants to adapt to environmental inputs. The regulation of auxin distribution in plant tissue is coordinately determined via multiple processes involved in auxin biosynthesis, polar transport from sites of synthesis, storage as inactive precursors, and the degradation of auxin (1–3). The major naturally occurring auxin, indole-3-acetic acid (IAA), is mainly biosynthesized from tryptophan by two sequential enzymatic steps involving TAA1, a tryptophan aminotransferase, and YUCCA, a flavin monooxygenase in the indole-3-pyruvic acid (IPA) pathway (4, 5). Molecular genetic studies in *Arabidopsis* have demonstrated that a combination of auxin transport proteins, comprising AUX1/LAX uptake permeases, the PINFORMED (PIN) efflux carriers, and ATP-binding cassette group B (ABCB) auxin transporters, coordinately regulates auxin transport (6). These transport proteins generate auxin gradients through the expression and subcellular relocalization of transport proteins in response to environmental and developmental cues (3). These multiple complicated processes coordinately regulate intra- and intercellular auxin distribution and ultimately determine the entire architecture of a plant. Thus, analysis and visualization of auxin distribution are essential to understand plant development.

SCF-type E3 ubiquitin-ligase complex (SCF^{TIR1})-based auxin-responsive reporters, such as *DR5::GFP* and *DII-VENUS*, are widely used to monitor auxin distribution in plants (7, 8). However, the spatiotemporal resolution of these reporter systems is limited due to the general nature of reporter protein expression and degradation. Alternatively, endogenous IAA distribution has been visualized through the direct detection of IAA molecules by means of immunostaining (9) and mass spectrometry-based IAA quantification (10). However, these direct-detection approaches require multiple and time-consuming procedures and present an insufficient spatial resolution of the IAA distribution at the cellular level. These direct and indirect approaches have illustrated an endogenous auxin distribution profile as the final output of the local biosynthesis, inactivation, and transport of auxin.

Here we developed fluorescent auxin analogs [7-nitro-2,1,3-benzoxadiazole (NBD)-conjugated naphthalene-1-acetic acid (NAA), NBD-NAA and NBD-IAA] that can be used to generate images of auxin distribution (Fig. 1*A*). These analogs were designed to function as active auxin analogs for the auxin transport system but to be inactive for auxin signaling. The analogs would be recognized as substrates by auxin transporters and then show a distribution pattern similar to auxin. This strategy of using fluorescent auxin analogs enabled the imaging of the auxin transport site and revealed the crucial role of local auxin synthesis in the formation of auxin maxima. Furthermore, these fluorescent analogs indicated the presence of a subcellular auxin gradient in plant cells.

Results

Design and Synthesis of Fluorescently Labeled Auxin Analogs. Fluorescently labeled forms of the plant hormones gibberellin, strigolactone, and brassinosteroid were recently generated for analysis

Significance

Fluorescent auxin analogs are designed to function as active auxins for the auxin transport system but to be inactive for auxin signaling. These fluorescent auxin analogs can mimic auxin via the transport system and be used to visualize inter- and intracellular auxin distribution in roots. These analogs allow imaging of auxin transport sites with high spatiotemporal resolution. Our fluorescent auxin system provides insight into auxin transport dynamics and subcellular auxin distribution.

Author contributions: K.H., T.N., A.S.M., and H.N. designed research; K.H., S.N., S.F., M.K.J., H.M., M.F., and T.A. performed research; K.H., A.S.M., H.M., M.F., and T.A. analyzed data; and K.H., S.N., M.K.J., A.S.M., and T.A. wrote the paper.

The authors declare no conflict of interest.

This article is a PNAS Direct Submission.

[1]To whom correspondence should be addressed. Email: hayashi@dbc.ous.ac.jp.

This article contains supporting information online at www.pnas.org/lookup/suppl/doi:10.1073/pnas.1408960111/-/DCSupplemental.

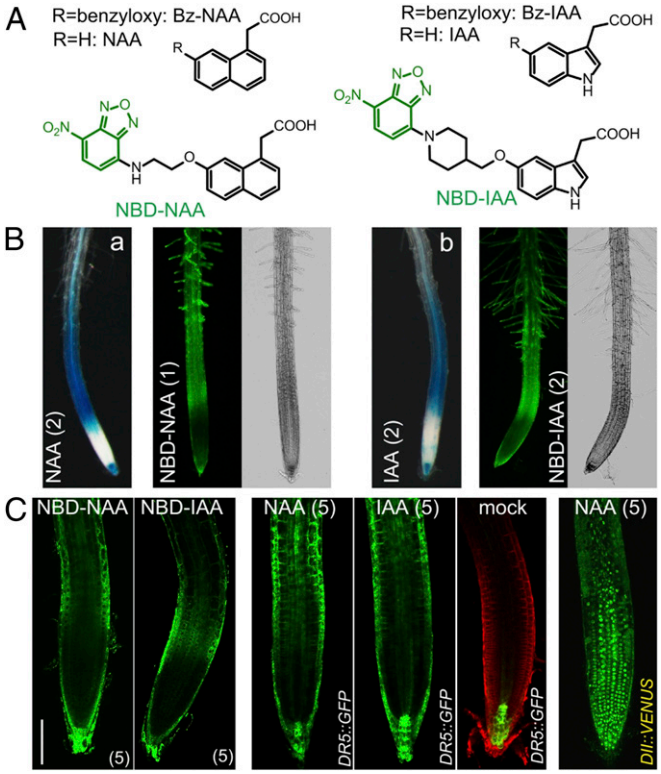

Fig. 1. Distribution of fluorescent auxin analogs in *Arabidopsis* root. (*A*) Structures of the auxins NAA and IAA and their fluorescent analogs NBD-NAA and NBD-IAA. (*B* and *C*) Distribution of NBD-auxins in *Arabidopsis* roots. Six-day-old wild-type seedlings were treated with medium containing NBD-auxins for 15 min. Six-day-old *DR5::GUS* (*B*, *a* and *b*) and *DR5::GFP* seedlings (*C*) were incubated with auxins for 4 h or 6 h, respectively. Six-day-old *DII-VENUS* seedlings were treated with 10 μM auxinole for 6 h and then incubated with NAA for 10 min. The pictures in *C* are confocal images. The values presented in parentheses indicate the concentration of chemicals (μM). (Scale bar, 100 μm.)

of the distribution of hormones and receptors (11–16). These fluorescently labeled hormones were designed to retain the original hormonal activity and to activate signaling by binding to hormone receptors (11–16). Under our strategy for design of fluorescent auxin analogs, the analogs undergo auxin transport in the same manner as native auxin molecules but are completely inactive for the signaling machinery. Auxins rapidly induce auxin-inactivating enzymes, such as GH3, and influence their own transport by regulating the localization of PIN proteins at the plasma membrane (3, 17). Similarly, active auxin analogs will immediately affect the localization of PIN and GH3 enzymes, and the distribution of the labeled analogs will therefore no longer reflect the native auxin gradient. According to our strategy for developing fluorescent auxin analogs, the analogs should satisfy the following criteria: First, they should be selective for auxin transporters, but not for the TIR1–Aux/IAA auxin receptor complex; and second, the overall polarity of the fluorescent auxin molecules should be as similar to that of native auxin molecules as possible. Lipophilic analogs would be free to travel across the plasma membrane and would therefore not establish a concentration gradient, thus showing a uniform distribution.

We recently reported that the alkoxy-auxin analogs Bz-IAA and Bz-NAA function as potent competitive inhibitors of the auxin transporters AUX1, PIN, and ABCBs (Fig. 1*A*) (18). These alkoxy-auxin analogs are inactive at auxin receptors but are recognized as auxin by auxin transporters. A structure–activity analysis revealed that auxin transporters ignore the alkoxy-chain substructure of auxin analogs (18). Based on our previous findings, we synthesized 5-fluorescently labeled IAAs and 7-fluorescently labeled NAAs as analogs of IAA and NAA, respectively (Fig. 1*A* and *SI Appendix*, Fig. S1). The artificial auxins NAA and Bz-NAA were efficiently exported by efflux transporters but were not imported by the AUX1 influx symporter, suggesting that fluorescent NAA analogs can be used to visualize efflux transport via PINs and ABCBs (18). The BODIPY and NBD fluorescent dyes were introduced into 5-hydroxy-IAA and 7-hydroxy-NAA using various alkyl linkers (*SI Appendix*, Fig. S1). Additionally, fluorescently labeled indole (NBD-indole) and benzoic acid (NBD-benzoic acid) were synthesized as negative controls to confirm the specificity of the fluorescence images of the auxin analogs (*SI Appendix*, Fig. S2*A*). The fluorescent gradient mimicking the auxin distribution should disappear when using negative control analogs if the transporters specifically recognize the auxin substructure of the fluorescent analogs. The fluorescent analogs were initially evaluated according to the fluorescence images they generated in comparison with the expression pattern of the *DR5* reporter in auxin-treated roots (Fig. 1*B*). Two of the tested fluorescent auxin analogs, NBD-IAA and NBD-NAA, represented analogs of the natural auxin IAA and synthetic auxin NAA, respectively, and produced similar fluorescence images compared with *DR5* reporter expression. The exogenously applied NBD-NAA and IAA (NBD-auxins) were preferentially accumulated in the root cap and elongation zone but not in the meristematic zone. These fluorescence images of NBD-auxins were similar to the exogenous auxin response profile of *DII-VENUS* (Fig. 1*C* and *SI Appendix*, Fig. S3). In contrast to NBD-auxins, the negative controls NBD-benzoic acid and NBD-indole showed faint, uniform fluorescence in the root (*SI Appendix*, Fig. S2*B*), suggesting that the auxin substructure is required for the *DR5* reporter-like distribution of NBD-auxin analogs.

Fluorescent Auxin Functions as an Auxin Analog Specific for Auxin Transport. We next assessed the effects of the fluorescent auxin analogs on auxin signaling and metabolism. To examine whether the fluorescent auxins were inactive in the SCF^{TIR1} pathway, *Arabidopsis* auxin-responsive reporter lines, including the synthetic auxin-responsive *BA3::GUS* (19) and *DR5::GUS* lines and native *pIAA3::GUS* and *pIAA12::GUS* lines (20), were incubated with NBD-auxins. Neither NBD-IAA nor NBD-NAA affected auxin-regulated reporter gene expression (Fig. 2 and *SI Appendix*, Fig. S4*A*), indicating that the fluorescent analogs are inactive regarding the modulation of early auxin-responsive gene expression. To further confirm that the fluorescent auxins are inactive as ligands of TIR1/AFB–Aux/IAA receptor complexes, we examined the binding of NBD-auxins to the TIR1–Aux/IAA receptor complex using a yeast two-hybrid system (21). In this system, IAA promotes the interaction between TIR1-DBD and Aux/IAA (IAA7)-AD to rescue *LEU2*-deficient yeast growth (Fig. 2*C*). NBD-auxins did not affect yeast growth in the absence or presence of IAA, suggesting that NBD-auxins do not bind to the TIR1 receptor. Calculations of molecular docking further indicated that NBD-auxins were inactive ligands for TIR1 receptor and auxin-binding protein 1 (ABP1) due to the larger molecular size of the analogs with respect to the auxin-binding cavity (*SI Appendix*, Fig. S4). These findings demonstrate that the fluorescent auxin analogs, NBD-auxins, are inactive in SCF^{TIR1} auxin signaling. The *Arabidopsis* early auxin-responsive gene *GH3* encodes an auxin-amino acid–conjugating enzyme that plays a central role in the modulation of endogenous auxin levels (22). GH3.6 recognizes both IAA and NAA as substrates and converts them to amino acid conjugates. To investigate whether the GH3 enzyme metabolizes the fluorescent auxins in vivo, fluorescence images of NBD-auxins were obtained in *GH3.6*-overexpressing (GH3ox) plants (*SI Appendix*, Fig. S5*A*). The fluorescence images of NBD-auxin would be expected to be altered in the GH3ox line if the analogs were rapidly converted to nontransportable amino acid conjugates. However, in GH3ox roots, the fluorescence images of the analogs were not altered, suggesting that the fluorescent auxins were not suitable substrates for the GH3 enzyme (*SI Appendix*, Fig. S5*B*). To further assess the stability of NBD-auxin, tobacco BY-2 cells were

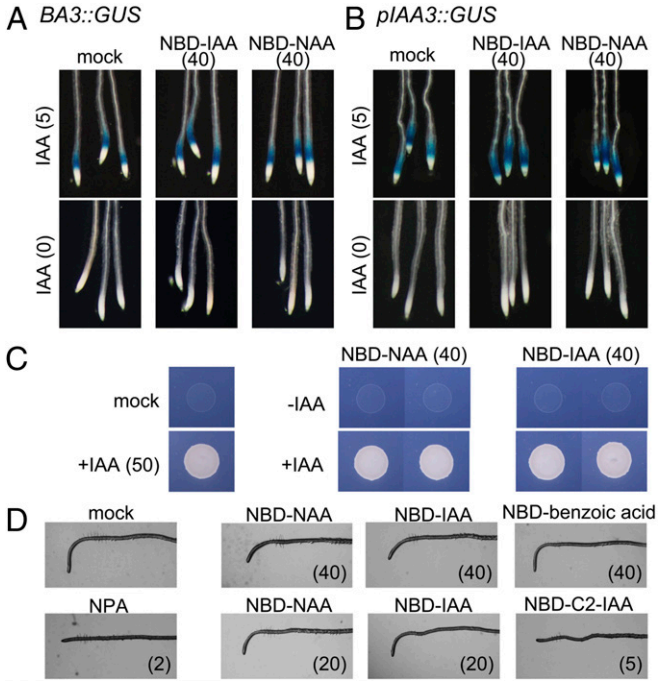

Fig. 2. Effects of NBD-auxins on SCF^{TIR1} auxin signaling. (*A* and *B*) Effects of NBD-auxins on auxin-responsive reporter gene expression. Six-day-old *BA3::GUS* (*A*) and *pIAA3::GUS* (*B*) lines were incubated with or without IAA, together with NBD-auxins, for 5 h or 16 h, respectively. (*C*) Yeast two-hybrid assay in which TIR1-DBD and Aux/IAA(IAA7)-AD fusion proteins were expressed. IAA enhanced the interaction between TIR1 and Aux/IAA to rescue *LEU2*-deficient yeast growth. (*D*) Effect of NBD-labeled analogs on the root gravitropic response. Roots (6-d-old) were placed on GM agar plates containing chemicals and grown in the dark for 5 h after rotating the plates at a 90° angle against the vertical direction. The values in parentheses indicate the concentrations of chemicals (μM).

incubated with NBD-NAA and its cellular metabolites were analyzed via fluorescence HPLC. The cellular NBD-NAA level was maintained, and the resultant fluorescent chromatograms were not altered after 50 min of incubation (*SI Appendix*, Fig. S5*C*).

In a previous study, we found that Bz-IAA and Bz-NAA inhibited root gravitropism by competing with the transport of endogenous auxin (18). IAA and NAA have been reported to reduce the root gravitropic response (23). We next studied the inhibitory activity of the fluorescent analogs against root gravitropism (Fig. 2*D*). NBD-auxins inhibited root gravitropism at a concentration of 40 μM, whereas NBD-benzoic acid did not. However, NBD-IAA and NBD-NAA were less active than the previously reported Bz-NAA and the auxin transport inhibitor 1-*N*-naphthylphthalamic acid (NPA) (Fig. 2*D* and *SI Appendix*, Fig. S6*C*). Although membrane-permeable analogs, such as Bz-NAA, are exported outside the cell, the subcellular concentration of diffusible Bz-NAA is maintained via simple diffusion. Thus, diffusible analogs would be expected to exhibit higher inhibitory activity than NBD-auxins. Accordingly, BOC-C2-NAA, a lipophilic analog of NBD-NAA, caused potent inhibition of gravitropism but was inactive to signaling, similar to Bz-NAA (*SI Appendix*, Fig. S6 *C* and *D*). Additionally, another diffusible fluorescent auxin, NBD-C2-IAA, showed a uniform fluorescent signal in the roots and inhibited gravitropism to a greater extent than NBD-IAA, as expected (*SI Appendix*, Fig. S6). This evidence indicated that the fluorescent auxin analogs are recognized by the auxin transport system as active auxin analogs but are inactive regarding auxin signaling and the metabolic pathway.

Auxin Transport System Regulates the Distribution of Fluorescent Auxin. To examine whether the auxin transport system establishes an asymmetric distribution of NBD-auxin analogs, we observed the distribution profiles of the analogs in the auxin transport mutant *pin2*, PIN1-overexpression lines (*35S::PIN1*), and wild-type plants treated with auxin transport inhibitors. Exogenous auxin strongly induced the expression of *DR5* reporters in the root elongation zone (Fig. 3*A*). Cotreatment with auxin transport inhibitor 2,3,5-triiodobenzoic acid (TIBA) blocked IAA movement, and *DR5* reporters were consequently expressed throughout the root tip, including in the meristematic zone (Fig. 3*A*). NBD-NAA was uniformly distributed in the *pin2* mutant, *35S::PIN1*, and wild-type plants treated with the auxin transport inhibitors brefeldin A, TIBA, NPA, and Bz-NAA (Fig. 3*B* and *SI Appendix*, Figs. S7 and S8). Additionally, the asymmetric distribution of NBD-NAA disappeared in the presence of excess IAA and NAA, but benzoic acid and 2-naphthoic acid did not affect the distribution of NBD-NAA. Similarly, the asymmetric distribution of NBD-IAA was abolished by excess amounts of NAA and auxin transport inhibitors. Furthermore, IAA and Bz-IAA decreased the fluorescent signal of NBD-IAA via competitive inhibition of auxin import. NBD-IAA signal was also reduced in the *aux1-7* auxin influx transport mutant (24), but NBD-NAA signal was not affected (*SI Appendix*, Fig. S9). NBD-NAA was able to bypass the AUX1 importer in the same manner as NAA (24). Consistent with the transport profile of alkoxy-auxins, these results suggest that NBD-auxins show the same transport profile as the original IAA and NAA molecules. Other mutants, for the auxin efflux transporters *abcb1*, *abcb19*, *pin3*, and *pin3 pin7* (6), did not show a dramatically altered distribution image of NBD-auxins in the roots (*SI Appendix*, Fig. S9). This altered distribution of NBD-auxins was observed only in the agravitropic roots in *pin2*, *35S::PIN1*, and *aux1-7* mutants. We

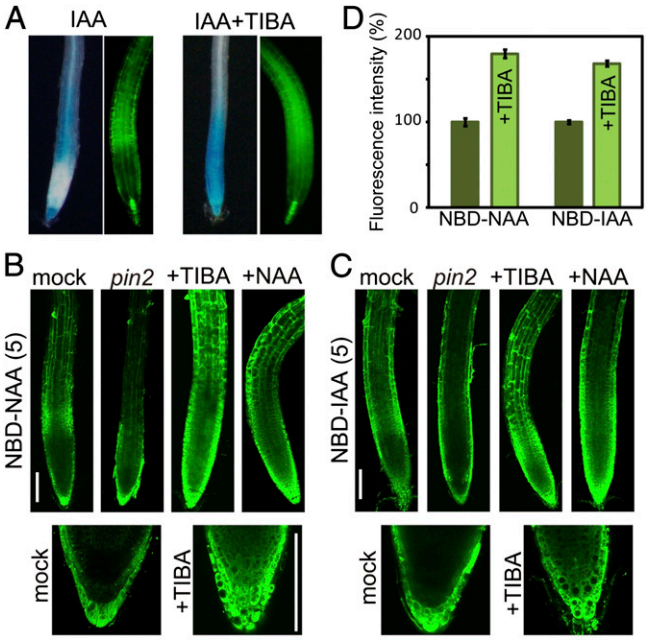

Fig. 3. Auxin transport system affects the distribution of fluorescent auxin in roots. (*A*) Effects of auxin transport inhibitors on the auxin-responsive *DR5* expression profile. Six-day-old *DR5::GUS* (*Left*) and *DR5::GFP* (*Right*) lines were treated with or without 20 μM TIBA, together with 2 μM IAA, for 5 h or 8 h, respectively. (*B* and *C*) Wild type (Columbia-0) and *pin2/eir1-1* mutants were treated with 5 μM NBD-auxins for 15 min. Wild-type roots were preincubated with 20 μM TIBA or 50 μM NAA for 4 h and 30 min, respectively, and then treated with 5 μM NBD-auxins, together with TIBA and NAA, for 15 min. The values presented in parentheses indicate the concentration of chemicals (μM). (Scale bars, 100 μm.) (*D*) *Arabidopsis* MM1 cells were incubated with 2 μM NBD-auxins with or without 50 μM TIBA for 30 min after preincubation with TIBA for 3 h. NBD-auxins were extracted from the harvested cells using methanol and quantified with a fluorometer. Error bars represent SEM; $n = 6$.

further studied the accumulation of fluorescent auxin analogs using *Arabidopsis* cultured cells. Both NBD-auxins were accumulated in the cultured cells, but NBD-benzoic acid did not (*SI Appendix*, Fig. S10). Treatment with the auxin transport inhibitor TIBA and excess NAA promoted the accumulation of NBD-auxins within the cells by repressing the export of NBD-auxins (Fig. 3*D* and *SI Appendix*, Fig. S10). This evidence indicates that fluorescent auxins are transported by the auxin transport system in roots.

Distribution of Fluorescent Auxin at the Root Apex. Recent findings regarding auxin biosynthesis through the IPA pathway have indicated an important contribution of locally synthesized IAA to the formation of auxin maxima (10, 25). The *DR5* reporter system allows for the visualization of auxin levels as the sum of transported and locally synthesized auxin, whereas our system using NBD-auxins selectively displays the flow of auxin. To estimate the contribution of auxin transport to the formation of auxin maxima at the quiescent center (QC), we monitored the distribution of exogenously applied auxins in auxin-depleted seedlings. *DR5::GFP* reporter seedlings were grown on medium containing the auxin biosynthesis inhibitors kynurenine and yucasin to deplete endogenous auxin (Fig. 4) (26, 27). Combined treatment with the TAA1 and YUCCA inhibitors dramatically inhibited primary root growth (*SI Appendix*, Fig. S11 *B* and *C*), similar to the auxin-deficient phenotype observed in the *taa1 tar2* double mutant and the *yuc 3 5 7 8 9* quintuple mutant (5, 28). The *DR5::GFP* maxima at the root apex disappeared in auxin-deficient seedlings (Fig. 4*C* and *SI Appendix*, Fig. S11*A*). This impaired root growth was completely restored by exogenous auxins supplied from the medium. However, exogenous NAA failed to recover *DR5::GFP* expression at the QC region in auxin-deficient roots (Fig. 4*D* and *SI Appendix*, Fig. S11), but NAA enhanced *DR5* expression at the columella and lateral root cap of auxin-deficient roots, similar to the distribution profile of NBD-NAA in wild-type roots. Additionally, exogenously applied 2,4-dichlorophenoxyacetic acid (2,4-D) was unable to form auxin maxima at the columella and lateral root cap (*SI Appendix*, Fig. S11*A*). This result is consistent with evidence showing that auxin efflux transporters effectively transport IAA and NAA but not 2,4-D (29). These findings suggest that auxin transport and local biosynthesis coordinately determine the position of auxin maxima in the root apex.

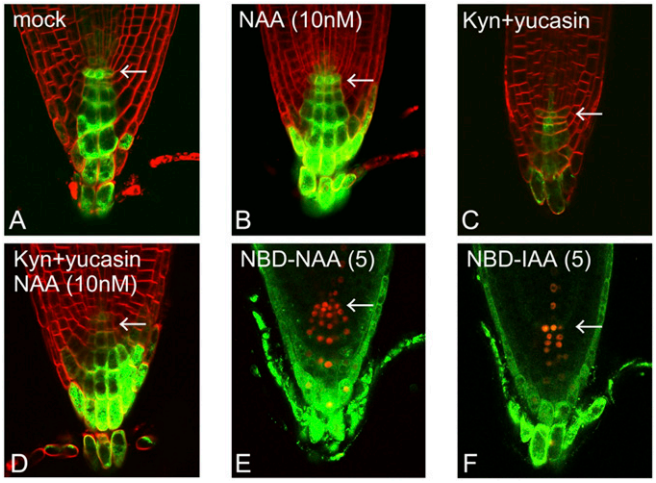

Fig. 4. Auxin maxima in the root apex. (*A–D*) *DR5::GFP* maxima in auxin-deficient roots. The *DR5::GFP* line was grown for 5 d on medium containing auxin biosynthesis inhibitors [10 μM kynurenine (Kyn) and 20 μM yucasin] with or without 10 nM NAA. (*E* and *F*) NBD-auxin distribution at the root apex in the *DR5::tdTomato*-NLS line. The values presented in parentheses indicate the concentration of chemicals (μM). The arrows indicate the QC region.

Fluorescent Auxin Distribution Mimics Native Auxin Accumulation in Vivo. Fluorescent NBD-auxin analogs are distributed to form an asymmetrical gradient in *Arabidopsis* roots. To examine whether the distribution of NBD-auxins mimics the endogenous auxin gradient in vivo, we analyzed fluorescence images of NBD-NAA in planta in different developmental stages and tissues and in response to environmental stimuli. At the very early seedling stage, seedlings treated with NBD-NAA showed similar fluorescence images as the *DR5::GFP* line (*SI Appendix*, Fig. S12). Polar transport of auxin is essential for lateral root formation, and auxin accumulates at high levels in the primordia of lateral roots (Fig. 5*A*) (9). NBD-auxins were selectively accumulated in the primordia of lateral roots and showed a similar pattern to *DR5::GFP* expression (Fig. 5 *A–C*). The development of the embryo is regulated by the asymmetric auxin distribution via PIN efflux carriers (7). NBD-NAA distribution showed a similar pattern to *DR5::GFP* expression in embryos (Fig. 5 *D* and *E*). Gravity signals regulate the auxin transport system to generate an asymmetric auxin distribution. Consistent with previous reports on the gravitropic response of the *DR5* reporter system (30), NBD-NAA was distributed on the elongated side of the hypocotyl, across gravistimulated hypocotyls (Fig. 5 *F* and *H*). In contrast, symmetric fluorescent signals were detected in vertically grown straight hypocotyl (Fig. 5*G*). To examine the transport of NBD-auxins in shoots, NBD-auxins were placed on the shoot apex and then incubated vertically. The distribution rate of NBD-auxin in the etiolated hypocotyl of the *pin3 pin7* mutant was slightly lower than the wild type (Fig. 5 *I* and *J* and *SI Appendix*, Fig. S13*A*). The fluorescent signal of NBD-auxins along the epidermal cells was clearly observed, and this transport of NBD-NAA was reduced by excess NAA and TIBA (*SI Appendix*, Fig. S13 *B* and *C*). However, NBD-auxins were less accumulated in the deeper cell layers or in the central cylinder (*SI Appendix*, Fig. S13 *C* and *D*), although the *DR5* reporter signal was shown in both the epidermal cells and the central cylinder (31). To confirm that the NBD-auxin distribution mimics the auxin gradient in other plant species, the distribution of NBD-NAA was observed in rice roots. In accordance with the distribution observed in *Arabidopsis* roots, NBD-NAA showed a similar pattern to the auxin-induced *DR5::GUS* response in rice roots (Fig. 5 *K* and *L*) (32).

Subcellular Distribution of Fluorescent Auxins. *DR5* and *DII-VENUS* auxin sensors allow for the clear visualization of intercellular auxin gradients in tissues. However, these SCF^{TIR1}-based systems are unable to visualize subcellular auxin gradients. In comparison, fluorescent auxin analogs display a high spatial resolution due to being small molecules. To investigate the subcellular auxin distribution, we initially visualized the distribution of subcellular NBD-auxins in tobacco BY-2 cultured cells. The auxin transport inhibitors NPA and TIBA induced the accumulation of cellular NBD-NAA, thus enhancing the fluorescent signal within a cell (Fig. 6 *A–C* and *SI Appendix*, Fig. S14). However, NBD-benzoic acid and NBD-indole did not exhibit clear signals in cultured cells (*SI Appendix*, Fig. S2*C*). Additionally, NBD-auxins were not colocalized with the tonoplast marker VHA-a3-mRFP (33) (*SI Appendix*, Fig. S15), suggesting that the localization of NBD-auxins was not due to the nonspecific binding of the NBD fluorophores to organelles or membranes. Several auxin transporters, such as PIN5, PIN8, and PILS, are subcellularly localized to the endoplasmic reticulum (ER) (34–36). NBD-auxin signals showed a similar localization pattern to the signals of PIN5-GFP and PIN8-GFP observed in BY-2 cells (Fig. 6 and *SI Appendix*, Fig. S14) (35, 37), and NBD-auxin signals colocalized well with the fluorescent signals from ER-Tracker. In the wild-type root, NBD-NAA accumulated at the root hair and colocalized well with ER-Tracker (Fig. 6 *G–L*). To further examine the subcellular distribution of NBD-auxins, the *Arabidopsis* root expressing the ER-retained CFP-HDEL protein (CFP-ER) was used. NBD-auxins were identically localized to CFP-HDEL (Fig. 6 *M–O* and *SI Appendix*, Fig. S16), confirming that NBD-auxin is preferably localized to the ER. The treatment of roots with TIBA highly

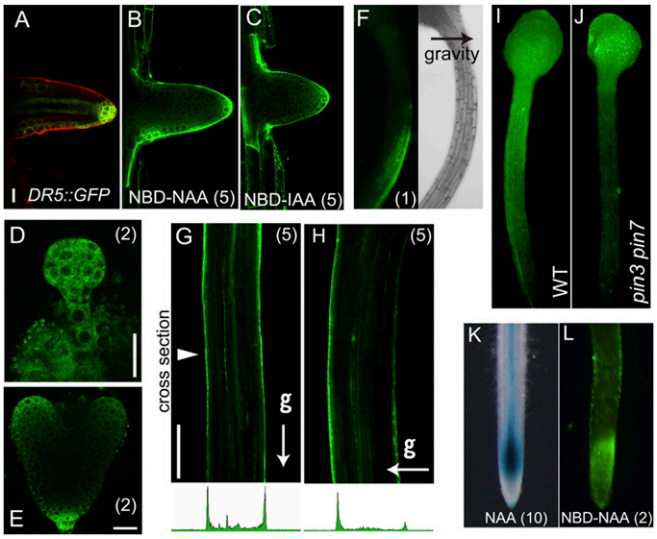

Fig. 5. Distribution of fluorescent auxin mimics the native auxin gradient. (*A–C*) *DR5*::GFP expression and fluorescent signals of NBD-auxins in lateral root primordia. (*D* and *E*) NBD-NAA distribution in preglobular embryos and heart-stage embryos. (Scale bars in *A–E*, 20 μm.) (*F–H*) Gravity-stimulated 3-d-old etiolated hypocotyls were treated with 1 μM NBD-NAA for 15 min (*F*) or 5 μM NBD-NAA (*G* and *H*) for 30 min while maintaining the unidirectional stimulus of gravity (g). Arrowhead indicates the cross section location. (Scale bar in *G* and *H*, 200 μm.) (*I* and *J*) Distribution of NBD-NAA in 4-d-old etiolated hypocotyls of wild type and *pin3 pin7* mutant. Agarose gel (0.1%, 0.2 μL) containing NBD-NAA (80 μM) was applied on the shoot apex and then incubated for 4 h in the dark. (*K* and *L*) Rice *DR5::GUS* roots were incubated with 10 μM NAA for 24 h (*K*). Distribution of NBD-NAA in rice roots (*L*). The values in parentheses indicate the concentrations of chemicals (μM).

accumulated NBD-NAA to form a steep gradient of NBD-NAA in the roots (*SI Appendix*, Fig. S16*C*). On the contrary, CFP-ER was uniformly distributed even in TIBA-treated roots. These results implied that NBD-auxins highly accumulate in the cytosol when auxin efflux transport is blocked.

Discussion

We herein demonstrate that fluorescently labeled auxin molecules are able to selectively monitor auxin transport sites. Our NBD-auxins displayed a similar auxin distribution image generated by SCF^{TIR1}-based sensors. The pharmacological and genetic evidence convincingly shows that the asymmetric gradient of NBD-auxins is established by the auxin transport machinery. Sokolowska et al. (38) recently reported fluorescently labeled IAA analogs to be active auxins. In these analogs, the fluorescent dyes fluorescein isothiocyanate (FITC) or rhodamine isothiocyanate (RITC) were directly conjugated to IAA at the indole NH group. These FITC/RITC-conjugated IAAs were reported to retain auxin-like activity in oat coleoptiles and *Arabidopsis* root (38), suggesting that these conjugated IAAs might be active toward TIR1/AFB–Aux/IAA receptor complexes. Our fluorescent auxin analogs are designed to be active in the auxin transport system but inactive for auxin signaling (*SI Appendix*, Fig. S2*B*), indicating that the concept of our auxin analogs is quite different from that of FITC/RITC-conjugated IAAs (38). The ABP1 and SCF^{TIR1} signaling pathways both affect the polar auxin stream by modulating the localization and abundance of PIN proteins at the plasma membrane (39, 40). Therefore, active analogs for auxin signaling can also impact auxin transport and hence disrupt the native auxin gradient. Previous studies have demonstrated that auxin biosensors, such as *DR5* reporters and the *DII-VENUS* system, display relative cellular IAA levels as the final output of IAA transport, biosynthesis, and metabolic pathways; however, their sensitivity is primarily governed by the expression of TIR1/AFB receptor proteins and their posttranscriptional regulation (41).

This study also demonstrated that local auxin biosynthesis plays a crucial role in the formation of auxin maxima in the QC region (Fig. 4). Petersson et al. demonstrated that de novo synthesized IAA accumulated at the root apex, thereby indicating that a source of IAA exists in the most apical region of *Arabidopsis* primary roots (10). Recent studies have shown that the expression of IAA biosynthesis genes is mainly localized near the QC region (25, 28, 42). Our fluorescent NBD-auxins were not accumulated in the QC region in our experimental conditions. NBD-auxins were incorporated from the surface of whole tissue and then distributed by the auxin transport system. This distribution process does not represent the native condition because endogenous IAA was locally supplied from specific auxin biosynthetic cells. Similar to the NBD-auxins, the *DR5* and *DII-VENUS* response images to exogenous auxin supported that auxin transport would not largely contribute to the formation of auxin maxima at the QC (Figs. 1*C* and 4*D*), confirming that NBD-auxins can mimic auxin transport sites at the root apex.

Our findings demonstrate the power of fluorescently labeled hormones designed to be selective for transport systems with a high spatial resolution. However, in the present work, we cannot discuss the kinetics and affinity of these labeled analogs in relation to distinct auxin transporters, such as PINs, ABCBs, and AUX1/LAX, due to the nonspecific binding of the analogs in the yeast system used for the alkoxy-auxin analogs (18). In the shoot, it seems that NBD-auxins were not efficiently transported by auxin transporters localized in the central cylinder (*SI Appendix*, Fig. S13). These results imply that NBD-auxins might aggregate locally at application sites; therefore, NBD-auxins are not versatile for the visualization of auxin transport streams in the shoot. Several ER-localized

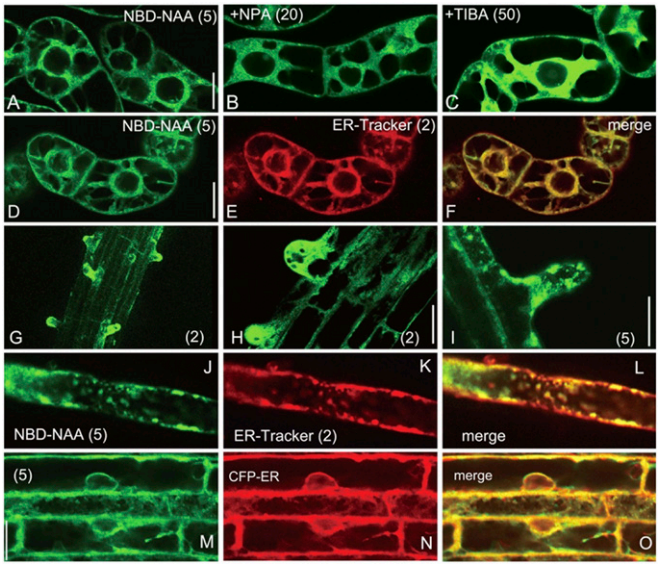

Fig. 6. Subcellular localization of NBD-NAA. (*A–C*) Auxin transport inhibitors NPA and TIBA facilitated the accumulation of subcellular NBD-NAA signals in tobacco BY-2 cells. The cells were preincubated with the auxin transport inhibitors NPA (*B*) or TIBA (*C*) for 4 h, and then NBD-NAA was added. The confocal images were recorded after a 20-min incubation. (*D–F*) Subcellular distribution of NBD-NAA in tobacco BY-2 cells. The cells were incubated with NBD-NAA (*D*) and ER-Tracker (*E*) for 20 min. (*G–I*) *Arabidopsis* roots were treated with NBD-NAA for 15 min, after which fluorescent confocal images were recorded. (*J–L*) Subcellular distribution of NBD-NAA in root hair. The root was cotreated with NBD-NAA (*J*) and ER-Tracker (*K*) for 20 min. (*M–O*) Subcellular distribution of NBD-NAA (*M*) in root cells expressing the ER marker (*N*) CFP-HDEL (CFP-ER). The root was treated with NBD-NAA for 20 min. The values in parentheses indicate the concentrations of chemicals (μM). (Scale bars, 20 μm.)

auxin transporters, such as PIN5, PIN8, and PILS, play a role in subcellular auxin homeostasis (34–36). Because of the general nature of small-molecule compounds, a small fraction of NBD-auxins might be passively diffused and nonspecifically bound to organelle membranes. Nevertheless, NBD-auxin robustly accumulated in the ER of *Arabidopsis* and tobacco cells, and cytosolic NBD-auxin levels were highly enhanced by auxin transport inhibitors. This evidence indicates that NBD-auxins can facilitate the visualization of the subcellular auxin gradient in cells.

Our fluorescent auxin analogs will provide insights into auxin biology in combination with multiple tools such as SCF^{TIR1}-based sensors (8, 35), pharmacological auxin probes (26, 27), and mathematical modeling (43).

Materials and Methods

Synthesis and Properties of Fluorescent Auxin Analogs. Full synthetic procedures and characterization of compounds are described in *SI Appendix, Materials and Methods*.

Plant Materials and Growth Conditions. *Arabidopsis thaliana* ecotype Columbia-0 was used as the wild-type control. Seeds were stratified for 2 d at 4 °C and cultured on germination medium (GM) (19) on soft gel plates (0.8 g/L gellan gum) or vertical agar plates (12 g/L agar) at 24 °C under continuous light for all assays. The mutant and transgenic *A. thaliana* lines used in this work are described in *SI Appendix, Materials and Methods*. *Arabidopsis* MM1 and tobacco cultured BY-2 cells were maintained on modified Murashige and Skoog (MS) medium on a rotary shaker (100 rpm) at 24 °C in the dark.

Imaging and Image Analysis. Fluorescence images were recorded with a fluorescence microscope (Olympus; BX-50) and a laser scanning confocal microscope (Olympus; FV-1200). Typically, the seedlings were incubated with half-strength MS medium containing NBD-analogs for 15–20 min at 24 °C in the dark, and fluorescence images were then immediately recorded. Complete methods are described in *SI Appendix, Materials and Methods*.

ACKNOWLEDGMENTS. We thank Drs. Hironori Kaminaka and Yoshiaki Inukai for providing materials, and Prof. Hyung-Taeg Cho and Dr. Hiroyuki Kasahara for critical reading of the manuscript. This work was funded by grants from the Japan Society for the Promotion of Science; Grant-in-Aid for Scientific Research (KAKENHI) 23510285 and 25114518 (to K.H.); and US Department of Energy, Chemical Sciences, Geosciences, and Biosciences Division, Basic Energy Sciences Grant DE-FG02-06ER15804 (to M.K.J. and A.S.M.).

1. Hayashi K (2012) The interaction and integration of auxin signaling components. *Plant Cell Physiol* 53(6):965–975.
2. Sauer M, Robert S, Kleine-Vehn J (2013) Auxin: Simply complicated. *J Exp Bot* 64(9): 2565–2577.
3. Petrásek J, Friml J (2009) Auxin transport routes in plant development. *Development* 136(16):2675–2688.
4. Mashiguchi K, et al. (2011) The main auxin biosynthesis pathway in *Arabidopsis*. *Proc Natl Acad Sci USA* 108(45):18512–18517.
5. Won C, et al. (2011) Conversion of tryptophan to indole-3-acetic acid by TRYPTOPHAN AMINOTRANSFERASES OF *ARABIDOPSIS* and YUCCAs in *Arabidopsis*. *Proc Natl Acad Sci USA* 108(45):18518–18523.
6. Peer WA, Blakeslee JJ, Yang H, Murphy AS (2011) Seven things we think we know about auxin transport. *Mol Plant* 4(3):487–504.
7. Friml J, et al. (2003) Efflux-dependent auxin gradients establish the apical-basal axis of *Arabidopsis*. *Nature* 426(6963):147–153.
8. Brunoud G, et al. (2012) A novel sensor to map auxin response and distribution at high spatio-temporal resolution. *Nature* 482(7383):103–106.
9. Benková E, et al. (2003) Local, efflux-dependent auxin gradients as a common module for plant organ formation. *Cell* 115(5):591–602.
10. Petersson SV, et al. (2009) An auxin gradient and maximum in the *Arabidopsis* root apex shown by high-resolution cell-specific analysis of IAA distribution and synthesis. *Plant Cell* 21(6):1659–1668.
11. Shani E, et al. (2013) Gibberellins accumulate in the elongating endodermal cells of *Arabidopsis* root. *Proc Natl Acad Sci USA* 110(12):4834–4839.
12. Irani NG, et al. (2012) Fluorescent castasterone reveals BRI1 signaling from the plasma membrane. *Nat Chem Biol* 8(6):583–589.
13. Rasmussen A, et al. (2013) A fluorescent alternative to the synthetic strigolactone GR24. *Mol Plant* 6(1):100–112.
14. Prandi C, et al. (2013) Strigolactone analogs as molecular probes in chasing the (SLs) receptor/s: Design and synthesis of fluorescent labeled molecules. *Mol Plant* 6(1): 113–127.
15. Bhattacharya C, et al. (2009) A new class of conjugated strigolactone analogues with fluorescent properties: Synthesis and biological activity. *Org Biomol Chem* 7(17): 3413–3420.
16. Prandi C, et al. (2011) New potent fluorescent analogues of strigolactones: Synthesis and biological activity in parasitic weed germination and fungal branching. *Eur J Org Chem* (20-21):3781–3793.
17. Löfke C, Luschnig C, Kleine-Vehn J (2013) Posttranslational modification and trafficking of PIN auxin efflux carriers. *Mech Dev* 130(1):82–94.
18. Tsuda E, et al. (2011) Alkoxy-auxins are selective inhibitors of auxin transport mediated by PIN, ABCB, and AUX1 transporters. *J Biol Chem* 286(3):2354–2364.
19. Oono Y, Chen QG, Overvoorde PJ, Köhler C, Theologis A (1998) age mutants of *Arabidopsis* exhibit altered auxin-regulated gene expression. *Plant Cell* 10(10): 1649–1662.
20. Weijers D, et al. (2005) Developmental specificity of auxin response by pairs of ARF and Aux/IAA transcriptional regulators. *EMBO J* 24(10):1874–1885.
21. Arase F, et al. (2012) IAA8 involved in lateral root formation interacts with the TIR1 auxin receptor and ARF transcription factors in *Arabidopsis*. *PLoS ONE* 7(8):e43414.
22. Ludwig-Müller J (2011) Auxin conjugates: Their role for plant development and in the evolution of land plants. *J Exp Bot* 62(6):1757–1773.
23. Ottenschläger I, et al. (2003) Gravity-regulated differential auxin transport from columella to lateral root cap cells. *Proc Natl Acad Sci USA* 100(5):2987–2991.
24. Marchant A, et al. (1999) AUX1 regulates root gravitropism in *Arabidopsis* by facilitating auxin uptake within root apical tissues. *EMBO J* 18(8):2066–2073.
25. Chen Q, et al. (2014) Auxin overproduction in shoots cannot rescue auxin deficiencies in *Arabidopsis* roots. *Plant Cell Physiol* 55(6):1072–1079.
26. He W, et al. (2011) A small-molecule screen identifies L-kynurenine as a competitive inhibitor of TAA1/TAR activity in ethylene-directed auxin biosynthesis and root growth in *Arabidopsis*. *Plant Cell* 23(11):3944–3960.
27. Nishimura T, et al. (2014) Yucasin is a potent inhibitor of YUCCA, a key enzyme in auxin biosynthesis. *Plant J* 77(3):352–366.
28. Stepanova AN, et al. (2008) TAA1-mediated auxin biosynthesis is essential for hormone crosstalk and plant development. *Cell* 133(1):177–191.
29. Seifertová D, et al. (2014) Characterization of transmembrane auxin transport in *Arabidopsis* suspension-cultured cells. *J Plant Physiol* 171(6):429–437.
30. Friml J, Wiśniewska J, Benková E, Mendgen K, Palme K (2002) Lateral relocation of auxin efflux regulator PIN3 mediates tropism in *Arabidopsis*. *Nature* 415(6873): 806–809.
31. Christie JM, et al. (2011) phot1 inhibition of ABCB19 primes lateral auxin fluxes in the shoot apex required for phototropism. *PLoS Biol* 9(6):e1001076.
32. Inukai Y, et al. (2005) Crown rootless1, which is essential for crown root formation in rice, is a target of an AUXIN RESPONSE FACTOR in auxin signaling. *Plant Cell* 17(5): 1387–1396.
33. Brüx A, et al. (2008) Reduced V-ATPase activity in the *trans*-Golgi network causes oxylipin-dependent hypocotyl growth inhibition in *Arabidopsis*. *Plant Cell* 20(4): 1088–1100.
34. Barbez E, et al. (2012) A novel putative auxin carrier family regulates intracellular auxin homeostasis in plants. *Nature* 485(7396):119–122.
35. Barbez E, et al. (2013) Single-cell-based system to monitor carrier driven cellular auxin homeostasis. *BMC Plant Biol* 13:20.
36. Barbez E, Kleine-Vehn J (2013) Divide et impera—Cellular auxin compartmentalization. *Curr Opin Plant Biol* 16(1):78–84.
37. Ganguly A, et al. (2010) Differential auxin-transporting activities of PIN-FORMED proteins in *Arabidopsis* root hair cells. *Plant Physiol* 153(3):1046–1061.
38. Sokolowska K, Kizinska J, Szewczuk Z, Banasiak A (January 7, 2014) Auxin conjugated to fluorescent dyes—A tool for the analysis of auxin transport pathways. *Plant Biol (Stuttg)*, 10.1111/plb.12144.
39. Baster P, et al. (2013) SCF(TIR1/AFB)-auxin signalling regulates PIN vacuolar trafficking and auxin fluxes during root gravitropism. *EMBO J* 32(2):260–274.
40. Sauer M, Kleine-Vehn J (2011) AUXIN BINDING PROTEIN1: The outsider. *Plant Cell* 23(6):2033–2043.
41. Parry G, et al. (2009) Complex regulation of the TIR1/AFB family of auxin receptors. *Proc Natl Acad Sci USA* 106(52):22540–22545.
42. Zhou W, et al. (2010) *Arabidopsis* tyrosylprotein sulfotransferase acts in the auxin/PLETHORA pathway in regulating postembryonic maintenance of the root stem cell niche. *Plant Cell* 22(11):3692–3709.
43. Band LR, et al. (2014) Systems analysis of auxin transport in the *Arabidopsis* root apex. *Plant Cell* 26(3):862–875.